A REFINED SENSOR MODEL FOR PANORAMIC CAMERAS

Jafar AMIRI PARIAN, Armin GRUEN

Institute of Geodesy and Photogrammetry
Swiss Federal Institute of Technology (ETH) Zurich
(parian, agruen)@geod.baug.ethz.ch

Keywords: Close Range Photogrammetry, Panoramic Camera, Sensor Modeling, Calibration, Tumbling/Wobbling Error, Accuracy

ABSTRACT:

Digital terrestrial panoramic cameras are providing a new device for taking high-resolution images. The produced images have been used widely for purely imaging purposes such as an indoor and landscape imaging, cultural heritage recording, tourism advertising and image-based rendering. Due to the high information content of those images they may also be used as an efficient means for 3D-object reconstruction. Therefore the need arises to establish a sensor model and investigate the potential of the system in terms of accuracy. With a well-defined sensor model we have additional powerful sensors for image recording and efficient 3D object modeling.
In this paper we present the result of physical measurements of tumbling for the SpheroCam. A method for tumbling error modeling of panoramic cameras is introduced and we will show how it can be used in bundle adjustment with additional parameters. Then we report the result of modeling and accuracy testing using a 3D testfield and compare it with the case when tumbling is not being modeled for EYESCAN and SpheroCam. The results indicate subpixel accuracy for both systems.

1. INTRODUCTION

The first panoramic cameras used in Photogrammetry were film-based aerial cameras. The Manual of Photogrammetry, 1966 lists a number of types, which differ mechanically and optically from each other. A prototype of an aerial panoramic camera can be modeled as a camera with a cylindrical focal surface, in which the image is acquired by sweeping a slit across this surface (Hartley, 1993). Through the integration of CCD technology, new types of airborne and terrestrial digital panoramic cameras were generated, using Linear Array CCDs as imaging devices. The EYESCAN jointly developed by German Aerospace Center (DLR) and KST Dresden GmbH and the SpheroCam, SpheronVR AG are two different types of line-based panoramic cameras. The EYESCAN camera is used in terrestrial photogrammetric applications was addressed in Scheibe, et al., 2001**.** Schneider and Maas, 2003 and Amiri Parian and Gruen, 2003 have worked on the mathematical modeling of panoramic cameras. Schneider and Maas investigated a geometrical model for a prototype of the EYESCAN panoramic camera and they performed calibration by using a 3D testfield and for 3D positioning they used intersection. Amiri Parian, Gruen have worked on a mathematical model of general line-based panoramic cameras. They performed calibration and accuracy test using a 3D testfield for EYESCAN and SpheroCam.

In this paper, we put emphasis on a mechanical error of a panoramic camera, causing tumbling. After a short review of the panoramic cameras, SpheroCam and EYESCAN, the mathematical sensor model is introduced. In chapter 4, the mathematical model of tumbling is introduced and chapter 5 gives the results of the physical measurement of the tumbling for the SpheroCam, and the calibration results of EYESCAN and SpheroCam with/without tumbling parameters. Finally, in this chapter we demonstrate the system accuracy for EYESCAN using a testfield.

2. PANORAMA TECHNIQUES

Several techniques have been used for panoramic imaging. Mosaicking or stitching, mirror technology, near 180 degrees (large frame cameras or one shot with fish-eye lens), and scanning 360 degrees (a new technology) are some known methods for panoramic imaging. Up to now, these techniques have been used for pure imaging, such as indoor imaging, landscape and cultural heritage recording, tourism advertising and image-based rendering, recently also for efficient Internet representations. Among the mentioned techniques for panoramic imaging, the last one has a possibility to produce a high-resolution panoramic image (more than 300 Mpixels) in one shot. The camera principle consists of a Linear Array, which is mounted on a high precision turntable parallel to the rotation axis. By rotation of the turntable, the linear array sensor captures the scenery as a continuous set of vertical scan lines.

In our tests we used a prototype of EYESCAN M3, a joint development between German Aerospace Center (DLR) and KST Dresden GmbH[*]. The camera is engineered for rugged everyday field use as well as for the measurement laboratory. The other digital panoramic camera used here is the SpheroCam from the SpheronVR AG[**], which operates similar to EYESCAN.

2.1. EYESCAN M3

Figure 1 shows the sensor system and Table 1 shows resolution parameters of the camera. The camera system contains three parts: camera head, optical part, and high precision turntable with a DC-gearsystem motor. The camera head is connected to the PC with a bi-directional fiber link for data transmission and camera control. The optical part of the system uses high performance Rhodenstock lenses. With adjustment rings one can use other lenses. The camera head is mounted on a high precision turntable with a sinus-commutated DC-gearsystem motor (Scheibe et al., 2001), internal motion control and direct controlling by the PC. Rotation speed and scan angle are pre-selectable and correspond to the shutter speed, image size and focal length of the lens. For a more detailed description see Schneider, Maas, 2003.

2.2. SpheroCam

The structure of the SpheroCam (Figure 1) includes 3 parts, the camera head, the optical part which is compatible with NIKON-lenses, and a DC motor to rotate the Linear Array. The SpheroCam is specially designed for use with a fish-eye lens, with a near 180° vertical field of view. As it rotates about its vertical axis, the SpheroCam then captures a complete spherical image. It is designed to capture high quality images. Table 1 contains resolution parameters of SpheroCam. For more detail on specifications of the camera see Amiri Parian, Gruen, 2003.

---

[*] http://www.kst-dresden.de/
[**] http://www.spheron.com/

Figure 1. Digital terrestrial panoramic cameras. EYESCAN (left) and SpheroCam(right)

Table 1. Parameters of EYESCAN and SpheroCam panoramic cameras

Resolution	EYESCAN	SpheroCam
Number of pixel in linear array (vertical resolution)	3600 or 10200 pixels per line	5300 pixels per line
Horizontal resolution (depends on the focal lens)	27489 pixels (35 mm lens)	39267 pixels (50 mm lens)
Pixel size	7 or 8 microns	8 microns

3. SENSOR MODEL

The sensor model as a mapping function is based on a projective transformation in the form of bundle equations, which map the 3D object space information into the 2D image space. The sensor model uses the following coordinate systems:

- Pixel coordinate system
- Linear Array coordinate system
- 3D auxiliary coordinate system
- 3D object coordinate system

Figure 2 shows the pixel coordinate (i, j) system. The original image observations are saved in this system. Figure 3 shows the other coordinate systems: Linear Array (0, y, z), auxiliary (X', Y', Z'), and object space (X, Y, Z) coordinate systems. The effects of lens distortion and the shift of the principal point are modeled in the Linear Array coordinate system. The rotation of the Linear Array and mechanical errors of the rotating turntable are modeled in the auxiliary coordinate system. The object space coordinate system is used as a reference for determining the exterior orientation parameters of the sensor.

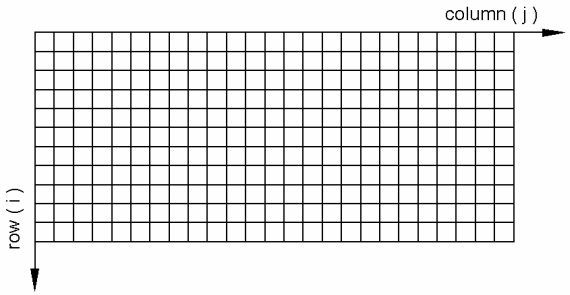

Figure 2. Pixel coordinate system (i,j)

To define the auxiliary coordinate system, an ideal panoramic camera is considered. Here the origin of the auxiliary coordinate system

coincides with the projection center O. The rotation axis passes through the projection center and coincides with Z'. X' passes through the start position of the Linear Array before rotation and Y' is defined to get a right-handed coordinate system.

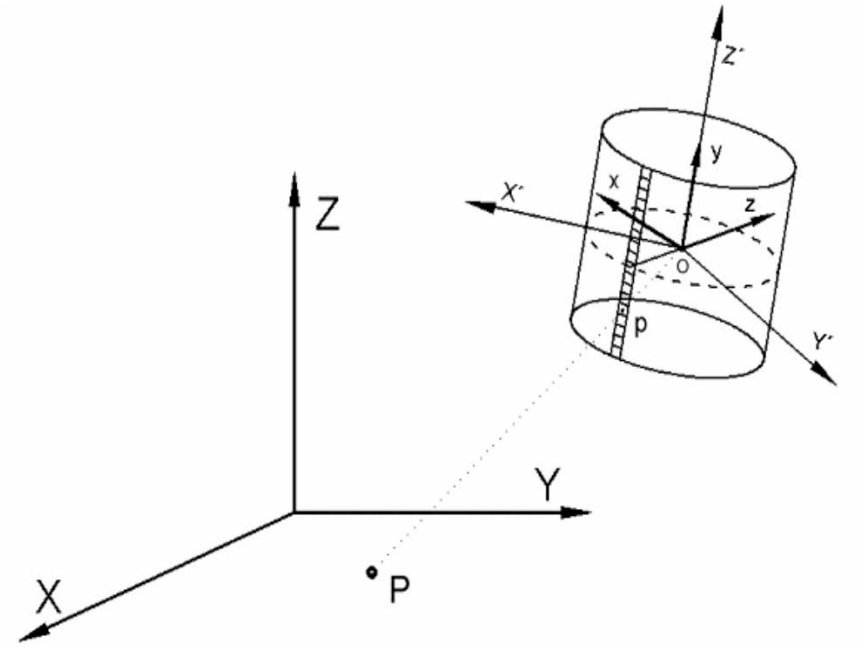

Figure 3. Object coordinate (X, Y, Z), auxiliary coordinate (X', Y', Z') and Linear Array (0, y, z) coordinate systems

The model, which directly relates pixel observations (i, j) to the object points (X, Y, Z), for an ideal sensor becomes (Amiri Parian and Gruen, 2003):

$$\begin{pmatrix} 0 \\ y \\ -c \end{pmatrix} = \lambda P^{-1} R_z^t(j\,A_h)\, M_{w,\varphi,k} \begin{pmatrix} X - X0 \\ Y - Y0 \\ Z - Z0 \end{pmatrix} \tag{1}$$

with

$$P = \begin{pmatrix} 0 & 0 & -1 \\ -1 & 0 & 0 \\ 0 & 1 & 0 \end{pmatrix} \qquad y = (i - \frac{N}{2})\, A_v$$

Where

A_h	Resolution of rotation
A_v	Pixel size of the Linear Array
c	Camera constant
N	Total number of rows or number of pixels in the Linear Array
R_z	3D rotation matrix around Z axis
P	Transfer matrix from the Linear Array to the auxiliary coordinate system
(0,y,-c)	Coordinates of image points in the Linear Array coordinate system
λ	Scale factor
$M_{w,\varphi,k}$	Rotation matrix
(X0, Y0, Z0)	Location of the origin of the auxiliary coordinate system in the object space coordinate system

There are many systematic errors disturbing the ideal model. The most important ones, with a distinct physical meaning are:

- Lens distortion
- Shift of principal point
- Camera constant
- Resolution of rotation
- Tilt and inclination of the Linear Array with respect to the rotation axis
- Eccentricity of the projection center from the origin of auxiliary coordinate system

Above errors were modeled as additional parameters for a prototype of a panoramic camera and the results of the modeling for two different cameras were reported in Amiri Parian, Gruen, 2003. However, in addition to the mentioned additional parameters, some systematic errors exist in the camera system. The most prominent one is tumbling, which shows its effect as a wobbling movement of the turntable and moves the origin of the auxiliary coordinate system. Next chapter describes the mathematical modeling of the tumbling error.

4. TUMBLING

Tumbling is mainly caused by an incomplete shape of ball bearings and the contacting surfaces (Matthias, 1961). The tumbling results from the mechanical properties of the instrument. Especially, it is affected by the rotation around the vertical axis and shows its effect as a change of the exterior orientation of the Linear Array during rotation. From that, one of the main effects of the tumbling is the moving of the origin of the auxiliary coordinate system during rotation (Figure 4).

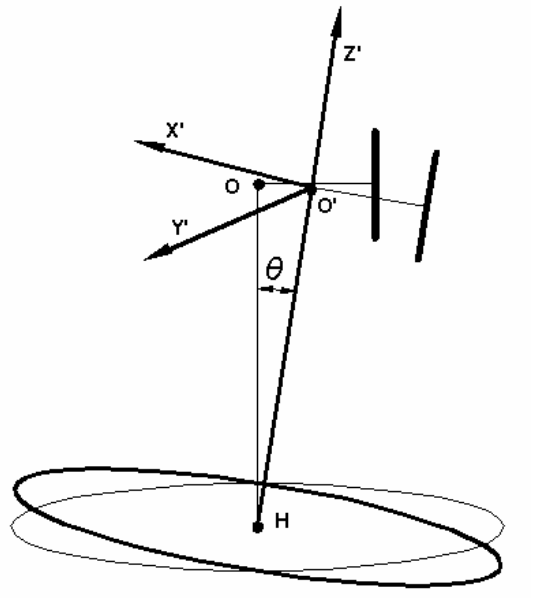

Figure 4. Effect of tumbling, Moving of the origin of the auxiliary coordinate system

Mechanically the physical rotation axis should represent a cylinder. If we suppose that this axis can be approximated locally by a mathematical straight line, then the turntable is constraint to have its oscillation around one point on the rotation axis and in the plane of the turntable. With this assumption we suppose that the turntable is constraint to oscillate around the center of the turntable H (Figure 4). Therefore tumbling can be represented as a rotation of the turntable around a 3D vector at the time of data acquisition. The mathematical formulation is presented by the concept of finite rotational axis (Quaternions or Euler's parameters).

A quaternion is defined as a complex number with one real part and 3 imagery parts:

$$q = q_1 + q_2 i + q_3 j + q_4 k$$

where (2)

$$i^2 = j^2 = k^2 = ijk = -1$$

And it can be used to represent a rotation about the unit 3D vector $\hat{n}$ by an angle θ (Arvo 1994, Hearn and Baker 1996):

$$q = (s, v) = (\cos(\frac{1}{2}\theta), \hat{n}\sin(\frac{1}{2}\theta)) \quad (3)$$

The four components of this quaternion are called Euler's parameters (4) describing a finite rotation about an arbitrary axis:

$$q_1 = \hat{n}_x \sin(\frac{\theta}{2}) \quad q2 = \hat{n}_y \sin(\frac{\theta}{2}) \quad q3 = \hat{n}_z \sin(\frac{\theta}{2}) \quad q4 = \cos(\frac{\theta}{2}) \quad (4)$$

Where, $\hat{n}_x, \hat{n}_y, \hat{n}_z$ are components of the unit vector $\hat{n}$.

A rotation matrix representing the tumbling of the turntable can be formulated by converting the Euler's parameters to the rotation matrix:

$$R_q = \begin{pmatrix} q_0^2 + q_1^2 - q_2^2 - q_3^2 & 2(q_1 q_2 + q_0 q_3) & 2(q_1 q_3 - q_0 q_2) \\ 2(q_1 q_2 - q_0 q_3) & q_0^2 - q_1^2 + q_2^2 - q_3^2 & 2(q_2 q_3 + q_0 q_1) \\ 2(q_1 q_3 + q_0 q_2) & 2(q_2 q_3 + q_0 q_1) & q_0^2 - q_1^2 - q_2^2 + q_3^2 \end{pmatrix} \quad (5)$$

In the case of a panoramic camera, $\hat{n}$ and θ are:

$$\begin{matrix} \hat{n} = \hat{n}(t) \\ \theta = \theta(t) \end{matrix} \quad \text{or} \quad \begin{matrix} \hat{n} = \hat{n}(j) \\ \theta = \theta(j) \end{matrix} \quad (6)$$

Where t is the time and j is the number of columns in the pixel coordinate system.

By inserting matrix (5) into the mathematical model of the sensor, the tumbling is modeled.
In the next chapter we will show, the physical measurement of the tumbling and the result of calibration and accuracy test using the tumbling parameters.

5. RESULTS

5.1. Physical measurement of the tumbling - SpheroCam

The examination of the tumbling error of SpheroCam was carried out by an inclinometer. In the present case, the Zerotronic from Wyler Switzerland is used, which provides the inclination in a specific direction. The inclinometer was placed firmly on the top of the turntable near the gravity center of the camera system. Then using the operating software of the camera, the inclinations of at least 3 continuous rotations (1080°) of the turntable at every 15° were recorded. To see whether the camera is stationary with respect to time, the measurements were carried out at 4 different epochs. Figure 5 shows the observations for one epoch. A Fourier analysis of the signal was carried out, which shows a high peak at the period π (Figure 5). The analysis of the other epochs shows that the camera is not stable over time. The instability of the camera causes different amplitudes and periods of the observations. Figure 6 shows the observations and the power spectrum of another epoch. These experiences indicate that the camera has a periodic oscillation. With that we defined functions $\theta(j)$ and $\hat{n}(j)$. In the next chapter we report the results of block adjustment with additional parameters and tumbling parameters.

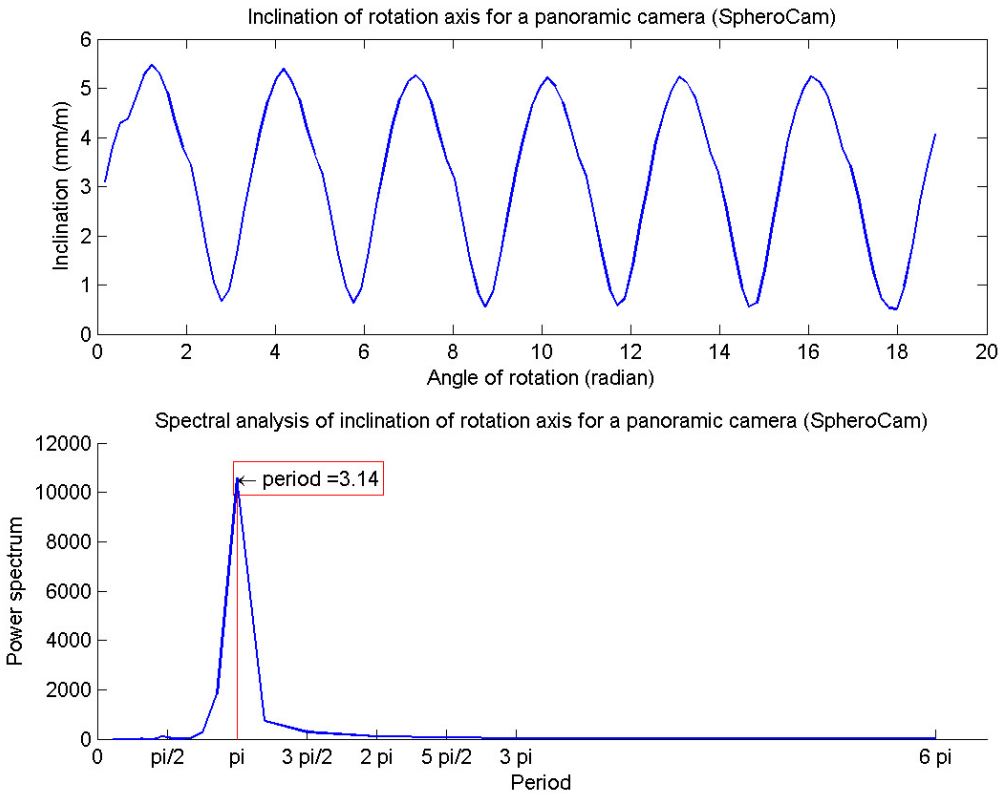

Figure 5. Observations for the inclination of the turntable (top) and the corresponding power spectrum (bottom) for epoch 1

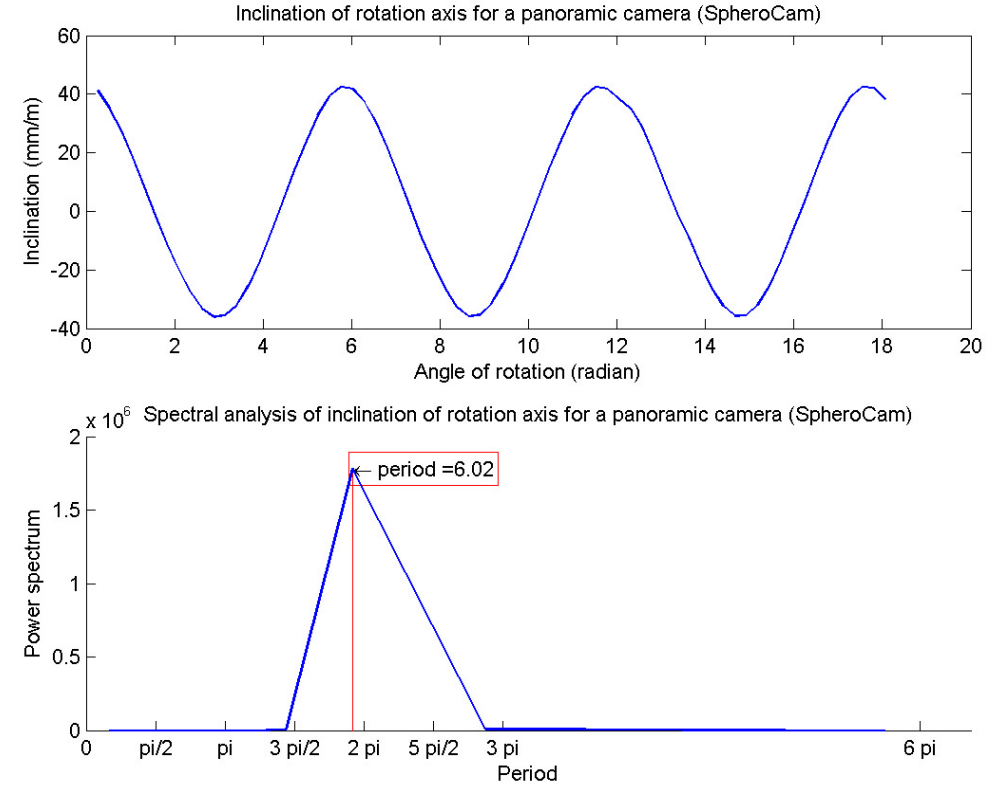

Figure 6. Observations for the inclination of the turntable (top) and the corresponding power spectrum (bottom) for epoch 2

5.2. Camera calibration considering the tumbling via additional parameters

Using the experience in the previous chapter we can consider $\theta(j)$ as a sin function with 3 parameters: amplitude, period and phase. In addition, we can define $\hat{n}(j)$ as the direction of the inclinometer's axis, which is in the plane that passes through the optical axis and the Linear Array. However, the inclination exists also on the other axes and can be modeled by another sin function with different 3 parameters.

5.2.1. SpheroCam

The camera calibration was performed using a testfield. We established a testfield with 96 circular targets at our institute and used it for the calibration of the SpheroCam. The testfield was measured with a Theodolite with mean precision of 0.3, 0.3, 0.1 mm for the three coordinate axes. To have a comparison of the effect of the tumbling parameters, at first a camera calibration was performed by all additional parameters mentioned at chapter 3, without the tumbling parameters. The a posteriori variance of unit weight is 1.37 pixels (10.9 microns). Figure 7 shows the image space residuals of the observations (the systematic pattern of the residuals is obvious).

In the second step, by adding the 6 parameters of tumbling errors for two perpendicular oscillations in the bundle adjustment, self-calibration was performed and the estimated posteriori variance of unit weight is 0.59 pixel (4.7 microns). Figure 8 shows the residuals of the observations in the image space for this case.

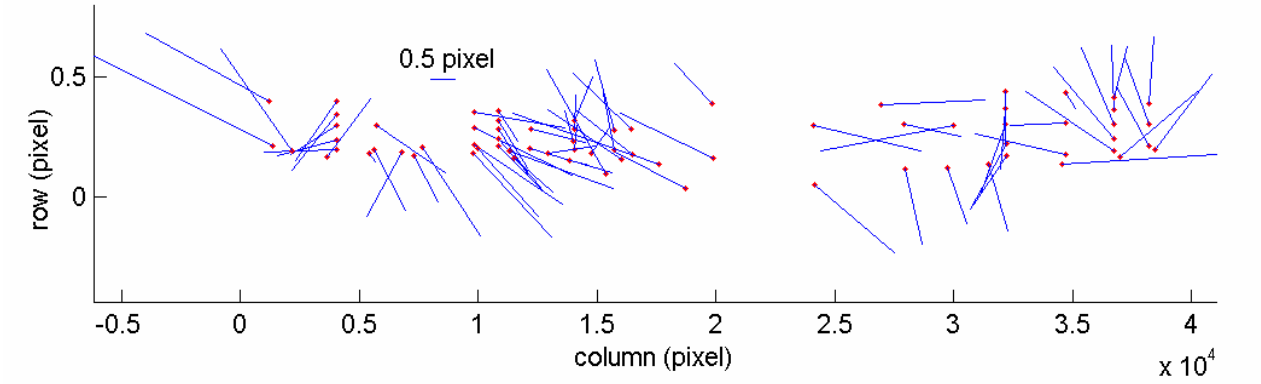

Figure 7. Image space residuals of the observation (without tumbling parameters)

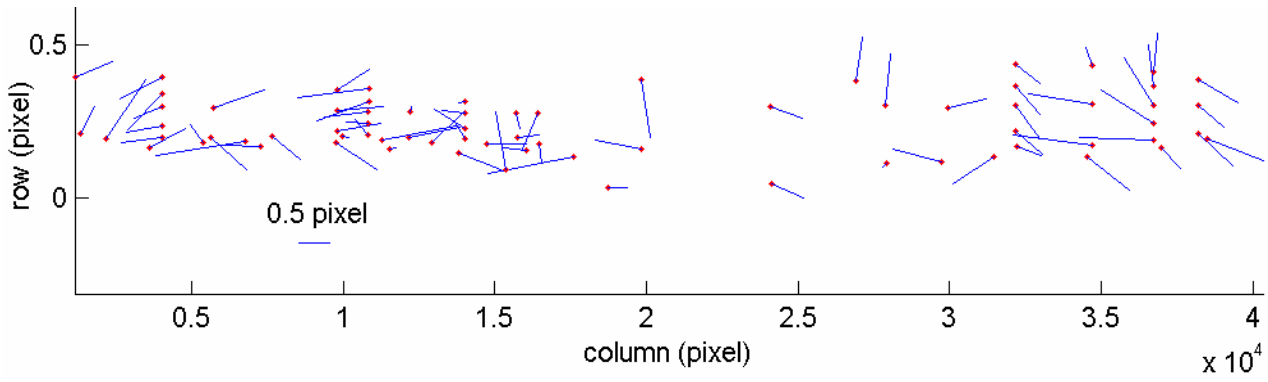

Figure 8. Image space residuals of the observation (with tumbling parameters)

5.2.2. EYESCAN

Since EYESCAN has also a turntable and operates like SpheroCam, it seems that it may have the same tumbling behavior. Therefore, we used the same model as was used for SpheroCam, but with a sin function with 3 parameters defining amplitude, period, phase.

For camera calibration, we got the image and field observations from Mr. Schneider, TU Dresden. TU's testfield consists of more than 200 control points and the mean precision is 0.2, 0.3, 0.1 mm for three coordinate axes. At first the camera calibration was performed with all additional parameters as mentioned at chapter 3 without tumbling parameters. The a posteriori computed variance of unit weight is 1.30 pixels (10.4 microns). Figure 9 shows image space residuals of the observations. A systematic pattern is obvious. In a second step we added 3 sin parameters for the tumbling error to the additional parameters. The a posteriori variance of unit weight is now 0.37 pixel (2.9 microns). Figure 10 shows the image space residuals of the observations, in which the systematic pattern of the residuals is enormously reduced.

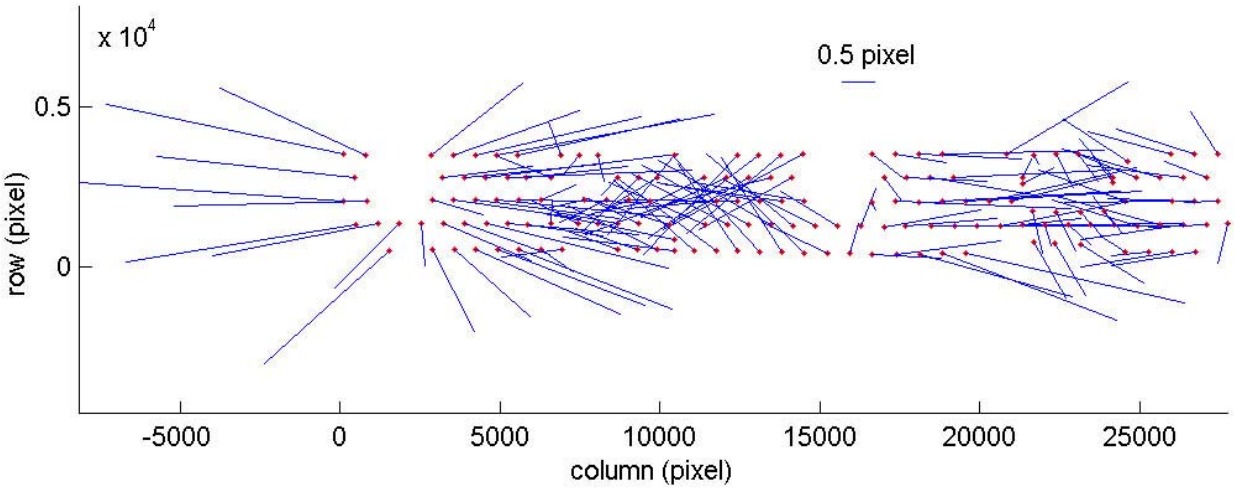

Figure 9. Image space residuals of the observations (without tumbling parameters)

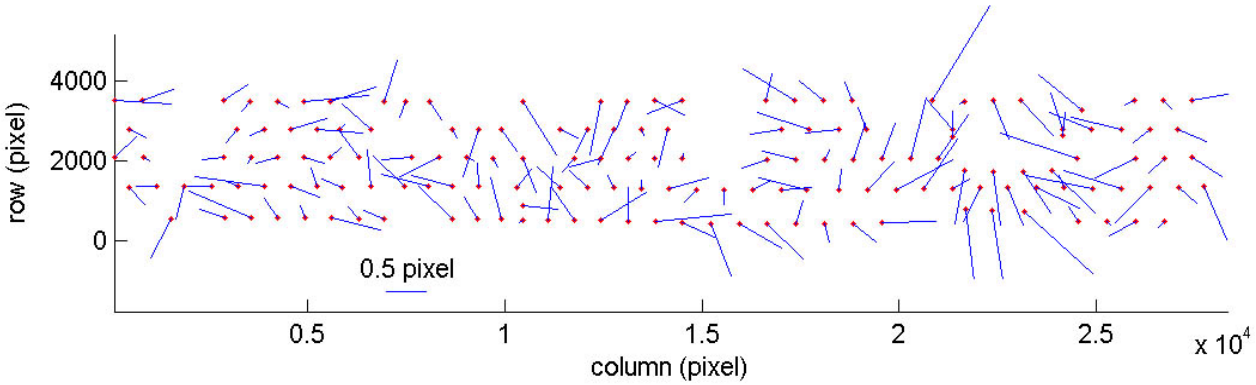

Figure 10. Image space residuals of the observations (with tumbling parameters)

5.3. Block adjustment with accuracy test - EYESCAN

An accuracy test was performed by block triangulation using 5 camera stations and by defining 140 check and 29 control points. Totally, 12 parameters were used as unknown additional parameters, considering tumbling parameters too. Figure 11 shows the object space residuals for checkpoints and Table 2 shows the results of adjustment. The estimated standard deviation of the image observations is 0.28 pixel, which is better than in the case of a single image.
For comparison a bundle adjustment was performed with 9 unknown additional parameters without tumbling parameters. The result of the adjustment (Table 2 and Figure 12) shows the object space residuals for checkpoints.

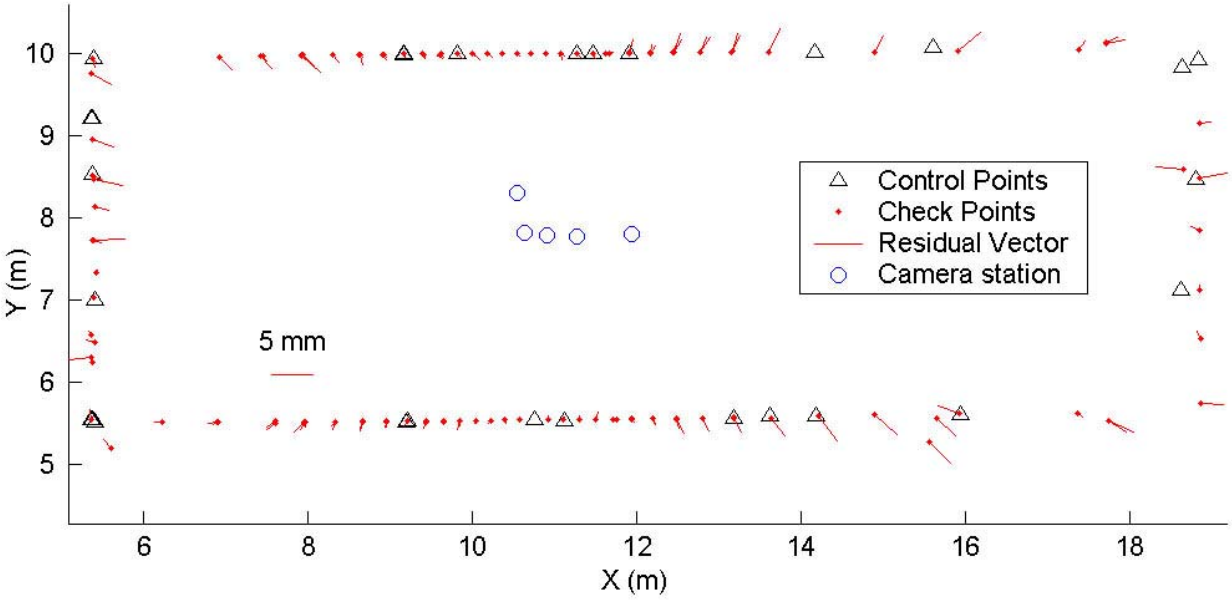

Figure 11. Object space residuals for check points (with tumbling parameters)

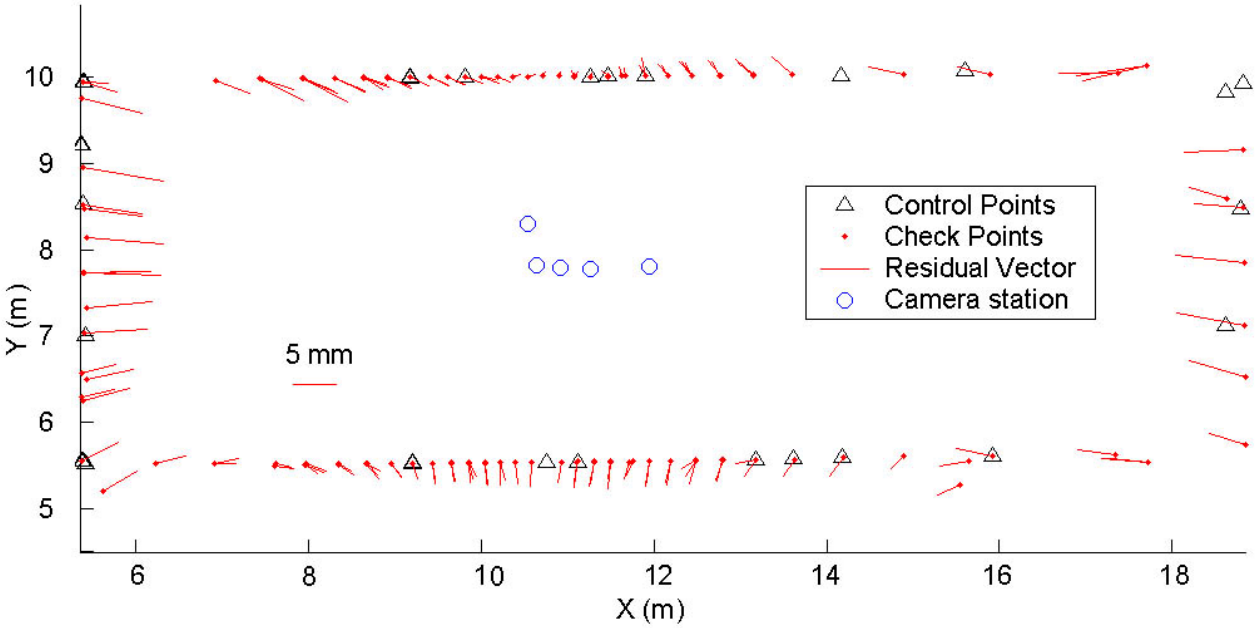

Figure 12. Object space residuals for check points (without tumbling parameters)

Table 2. Results of block adjustment – accuracy test

	With tumbling parameters (Figure 11)	Without tumbling parameters (Figure 12)
Number of Checkpoints	140	140
Number of Control Points	29	29
RMS Checkpoints (X,Y,Z) (mm)	1.16, 0.99, 0.52	3.14, 1.56, 0.85
STD Checkpoints (X,Y,Z) (mm)	2.39, 0.82, 0.77	4.61, 1.57, 1.48
$\hat{\sigma}_0$ (pixel)	0.28	0.54

6. CONCLUSION

We improved the sensor model by the modeling of the tumbling of the camera for two terrestrial panoramic cameras EYESCAN and SpheroCam. We measured the tumbling of the SpheroCam using an inclinometer. With this experience, we performed self-calibration by using all additional parameters (including tumbling parameters) for EYESCAN and SpheroCam. The estimated standard deviations for the observations in image space are 0.59 pixel for the SpheroCam and 0.37 pixel for the EYESCAN. An accuracy test was performed by defining 29 control points and 140 checkpoints. The achieved accuracy in object space is 1.16, 0.99, 0.52 mm for the three coordinate axes.

In this study we improved the mathematical model by adding 6 sin function parameters to model the tumbling error of the SpheroCam and 3 sin function parameters to model the tumbling error of the EYESCAN and with that the accuracy improved significantly. However, there are more mechanical errors in the instrument, which show its effect as a systematic pattern in the residuals. The modeling of these mechanical errors needs more parameter for $\theta(j)$ and different definitions for $\hat{n}(j)$. The reduction of the tumbling error of panoramic camera by the manufactures will certainly provide highly accurate optical measurement system.

Acknowledgements

We appreciate the cooperation of D. Schneider, TU Dresden, who provided us with the image coordinates and control point coordinates for the testing of the EYESCAN camera. We are also grateful to Prof. Dr. L. Hovestadt, ETH Zurich, who rented us his group's SpheroCam for testfield investigations.

References

Amiri Parian, J. and Gruen, A., 2003. A Sensor Model for Panoramic Cameras. In Gruen/Kahmen (Eds.), 6th Conference on Optical 3D Measurement Techniques, Vol. 2, pp. 130-141, Zurich, Switzerland.

Arvo, J., 1994. Graphics Gems II. New York: Academic Press, pp. 351-354 and 377-380.

Hartley, R., 1993. Photogrammetric Techniques for Panoramic Camera. SPIE Proceedings, Vol. 1944, Integrating Photogrammetric Techniques with Scene Analysis and Machine Vision. Orlando, USA, pp. 127-139.

Hearn, D. and Baker, M. P., 1996. Computer Graphics: C Version, 2nd ed. Englewood Cliffs, NJ: Prentice-Hall, pp. 419-420 and 617-618.

Manual of Photogrammetry, 1966. Third edition. American Society for Photogrammetry and Remote Sensing, pp. 145-156.

Matthias, H., 1961. Umfassende Behandlung der Theodolitachsenfehler auf vektorieller Grundlage unter spezieller Berücksichtigung der Taumelfehler der Kippachse. Verlag Leemann, Zürich.

Scheibe, K., Korsitzky, H., Reulke, R., Scheele, M., Solbrig, M., 2001. EYESCAN - A High Resolution Digital Panoramic Camera. Robot Vision: International Workshop RobVis 2001, Auckland, New Zealand. Volume 1998/2001, pp. 77-83.

Schneider D. and Maas H.-G., 2003. Geometric modelling and calibration of a high resolution panoramic camera. In Gruen/Kahmen (Eds.), 6th Conference on Optical 3D Measurement Techniques, Vol. 2, pp. 122-129, Zurich, Switzerland.